Bulgarian Journal of Physics vol. **XX** (20XX) 1–12

Interplanetary Coronal Mass Ejections: A Statistical Study of Solar Cycles 23 and 24

Hemlata Dharmashaktu[1] ✉, **Nawal Kishor Lohani**[2]

[1]S.S.M.M.U.S.S.S. Govt. P.G. College, Dwarahat, Almora, India
[2]M.B.G.P.G.C. Haldwani, Nainital, India

Received *23 September 2026*

Abstract. Interplanetary Coronal Mass Ejections (ICMEs) are among the most important drivers of geomagnetic storms (GMSs) and space weather disturbances at Earth. This study presents a statistical analysis of ICME characteristics during solar cycles (SC) 23 and 24 from 1996 to 2018, focusing on their occurrence, propagation properties, and geoeffectiveness. The results show a significant decrease in the total number of ICMEs during SC 24 compared to SC 23.

However, the fraction of magnetic clouds (MCs) increased from 41% in SC 23 to 64% in SC 24, while ejecta (EJ) and complex structures became less frequent. A total of 53 halo CME–ICME pairs associated with intense geomagnetic storms ($Dst \leq -100$ nT) were identified and classified into MC and EJ events. Most ICME-associated CMEs were halo events, and ICME speeds were generally concentrated near the ambient solar wind speed ($\sim$ 400–450 km/s).

ICME transit times ranged from 23 to 104 hours during SC 23, whereas the minimum transit time increased to about 43 hours in SC 24. Strong inverse correlations were observed between transit time and ICME speed for both MCs ($r = -0.81$) and EJs ($r = -0.77$). Shorter transit times were generally associated with stronger geomagnetic storms, particularly for MC events. Furthermore, MCs exhibited stronger correlations between the Dst index and interplanetary parameters, including IMF B_z ($r = 0.81$), IMF B ($r = -0.62$), and B_zV ($r = 0.85$), compared to EJs. These results indicate that MCs are generally more geoeffective than EJs and highlight the importance of ICME propagation characteristics and magnetic field properties in determining geomagnetic storm intensity.

KEY WORDS: Sun; CME; ICME; GMSs; Magnetic cloud; Ejecta.

1 Introduction

Coronal Mass Ejections (CMEs) and associated eruptive flares are the most violent manifestations of the active Sun. A flare is characterized by the rapid and impulsive release of a large amount of energy over a time scales of a few to several tens of minutes. On the other hand, CMEs are primarily the eruption of a substantial amount of plasma (approximately $10^{14} - 10^{16}$ g), huge amount of energy (approximately $10^{27} - 10^{32}$ ergs) with speeds ranging from 100 to up to 3300 km/s) from the Sun. During a CME, the large-scale eruption of plasma and magnetic field leads to significant alterations in the solar corona's magnetic configuration [1–3]. Interplanetary CMEs (ICMEs), are well known to be important drivers of enhanced geomagnetic activity, can cause non-recurrent geomagnetic storms when they collide with Earth's magnetic field, especially if they carry a strong and sustained southward magnetic field component [4, 5].

Early solar wind observations have confirmed that CMEs at 1 AU typically exhibit distinct plasma and field signatures, distinguishing them from the ordinary solar wind (see the review by [6]. ICMEs in the solar wind flow are characterized by unusually low proton and electron temperatures, bidirectional suprathermal electron strahls, and anomalies in plasma composition [7]. With continuous in-situ observations at 1 AU of multiple plasma and magnetic field parameters of the solar wind, it is now possible to identify Earth-directed ICMEs that correspond to CMEs launched from the Sun several hours earlier.

A subset of ICMEs identified by [7] charactersied by a low proton temperature and an enhanced magnetic field (> 10 nT) that smooth rotation of its components, resembling that of a flux rope. Such structures are referred to as Magnetic Clouds (MCs). The magnetic field configuration of MCs, as suggested by modelling, is associated with a magnetic flux rope. This interpretation aligns with the occasional detection of the helical structure of the CME in the corona and near-Sun region [8, 9]. However, it's important to note that typical features of an MC can be completely absent or only partially present in several ICMEs, indicating the complexity associated with the structural evolution of the CMEs. When MC features are absent, ICMEs are classified as Ejecta (EJ).

We particularly focus on the propagation characteristics of ICMEs, such as transit time and interplanetary speed, and their variations along different solar cycles. We further categorize ICMEs into two subsets – MCs and EJ, to explore how the observed ICME structures at 1 AU could be associated with the corresponding CME properties during the early evolution at the near-Sun region.

2 Data Sources and Methodology of the Analysis

The present analysis is primarily based on the catalogue compiled by Ian Richardson and Hilary Cane https://izw1.caltech.edu/ACE/ASC/DATA/level3/icmetable2.htm [10] and https://ustc.edu.cn as well as the catalogue of CMEs from the

Large Angle and Spectrographic Coronagraph (LASCO) onboard the Solar and Heliospheric Observatory (SOHO) of the CDAW Data Center at Goddard Space Flight Center https://nasa.gov [11]. The ICME catalogue also provides information on whether the observed ICME presents a Magnetic Cloud (MC) structure or not, based on the criteria proposed by Burlaga in 1981 [7, 12]. Study uses the same terminology to define two distinct classes of ICMEs, namely MC and EJ. The catalogue also notes complex events where the MC structures cannot be fully defined.

The data used in the study was obtained from the Omni web data center https://nasa.gov for the Dst, IMF B and B_z components, and solar wind speed (V). The average correlation coefficient was also calculated using cross-correlation analysis between the geomagnetic indices and ICME parameters for the respective years to identify the causes of geomagnetic activity.

3 Result and Discussion

In this study, we examined 218 pairs of ICME and CMEs that were linked with intense GMS having a $Dst \leq -50$ nT then divided them into three subsets: MCs, EJs and Complex (include only in the main list) during SC 23 and 24. Subsequently, we categorize all 53 halo CME-ICME pair into two distinct subsets, i.e. MCs and EJ that were associated with intense GMS, characterized by a $Dst \leq -100$ nT, during the periods of SC 23 and 24.

3.1 CME-ICME interaction

Table 1 presents the occurrence statistics of ICMEs and their three subsets: Magnetic Clouds (MCs), Ejecta (EJ), and complex events, during SC 23 and SC 24. A significant decrease in the number of ICMEs is observed in SC 24 compared to SC 23 (59 versus 159). Interestingly, the proportion of MC-type events out of the total ICMEs is considerably higher in SC 24 (64%) than in SC 23 (41%). Evidently, SC 24 has a much lower percentage of EJ and complex cases compared to the previous cycle.

Table 1. Occurrence of ICMEs during SC 23 and SC 24 for all kinds of events, such as magnetic clouds (MC), ejecta (EJ), and complex events

	Number of events			
Solar cycle	MC	EJ	Complex	Total
23	65	46	48	159
24	38	9	12	59

In Figure 1, we plot histograms of the initial speeds of CMEs and the corresponding speeds of the ICMEs for both SC 23 and SC 24. The comparison of

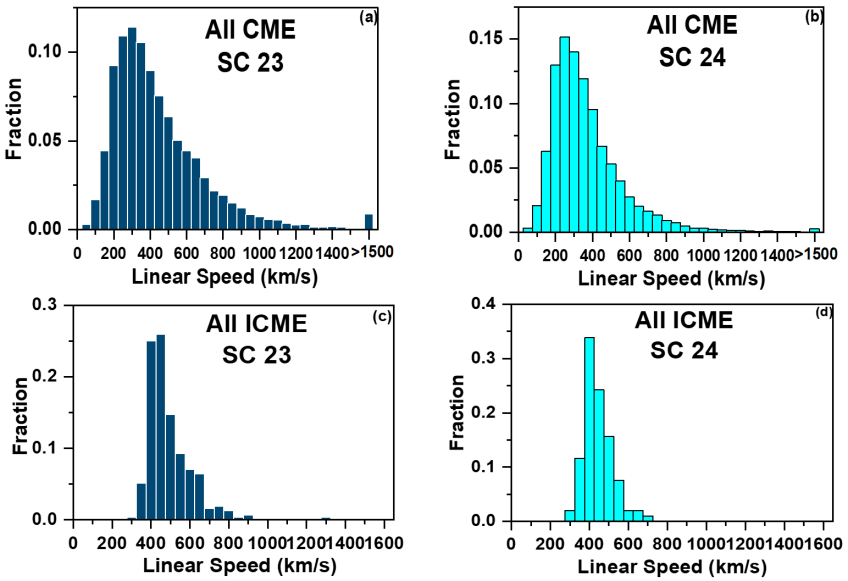


Figure 1. Upper panel: histograms of the initial speeds of all CMEs in the LASCO field of view for: (a) SC 23 and (b) SC 24. Lower panel: histograms of ICME speeds at 1 AU for: (c) SC 23 and (d) SC24.

near-Sun CME observations (Figures 1a and 1b) reveals that CMEs displayed a broad range of initial speeds in both cycles; however, SC 24 had fewer high-speed CMEs than SC 23. Conversely, the speed range of ICMEs is quite narrow (Figures 1c and 1d) and tends to distribute around the ambient solar wind speed (approximately 400—450 km/s). Most ICME–CME associations correspond to wide CMEs with angular extents of halo CME. Our results were in agreement with earlier findings of M. Syed Ibrahim.

3.2 Solar cycle variation and ICME

In Figure 2, we present a histogram of the total ICMEs (panel a), during SC 23 and SC 24. It is important to note that the annual rate of CMEs reaching the vicinity of Earth at 1 AU, represented as ICMEs is approximately 9 events per year. For comparison, we also display the histogram of the total annual CME counts and the plot of the yearly sunspot number during the same period in Figure 2b. For instance, when we take into account all the CMEs observed by LASCO during the same timeframe, the annual CME rate stands at 1290 events per year. An examination of histograms (a) and (c) reveals that the ICMEs reaching the near-Earth region form a very small fraction of the total CMEs originat-

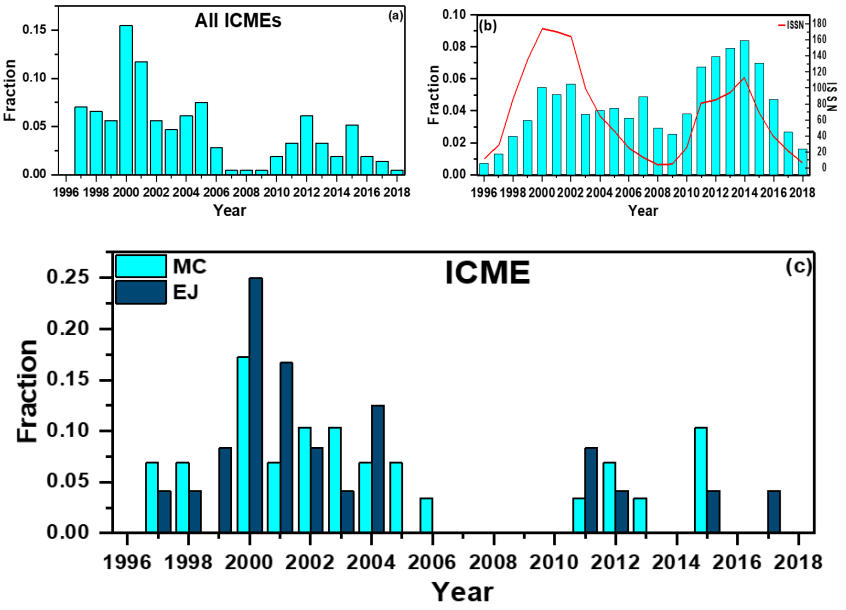


Figure 2. (a) Histograms showing the annual occurrence of all ICMEs during SC 23 and SC 24; (b) Histogram occurance of all CMEs seen in LASCO field of view for SC 23 and SC 24 and their variation with sunspot number (ISSN); (c) Two types of ICMEs (MC & EJ) for which $Dst \leq -100$ nT and are associated with halo CMEs. MCs (light blue) and EJs (dark blue), are shown for SC 23 and SC 24.

ing from the Sun. We note that although SC 24 being significantly weaker than its predecessor in terms of sunspot numbers, it exhibited a higher CME activity. The years 2000 and 2012 saw the highest number of ICMEs during SC 23 and 24, respectively, as shown in Figure 2a.

Since most of the ICME–CME associations correspond to wide CMEs with angular extents of halo CME, so we selected 53 ICME-halo CME pair for further analysis. Two categories of events are identified: MC events and EJ events. In Figure 2, we present a histogram of the ICMEs (panel c), along with MC and EJ events for which $Dst \leq -100$ nT, associated with halo CMEs during SC 23 and SC 24 (Table 2). The bar chart of MC and EJ events reveals intriguing variations in their temporal evolution across different phases of the solar cycles. Throughout SC 23, it has been observed that MCs are prevalent during the rise and decline phases of the solar cycle, whereas EJs surpass the yearly count during the maximum phase of the cycle. In contrast, throughout SC 24, MCs dominated during the maximum phase, whereas EJs were more prevalent during the rise and decline phases of the solar cycle.

Table 2. List of 53 CME-ICME pairs associated with GMS ($Dst \leq -100$ nT) and related parameters during SC 23 and 24

LASCO CME	Time	CME speed	ICME sta11	Time	ICME speed	ICME type	B_z (nT)	B (nT)	Dst (nT)	CME location
05/12/1997	5:30	464	05/15/1997	9:00	450	MC	-24.2	21	-115	N21W08
11/04/1997	6:10	1556	11/07/1997	4:00	400	MC	-12.9	11	-110	S18W63
05/02/1998	14:06	938	05/04/1998	10:00	550	EJ	-29	10	-205	S15W15
10/15/1998	10:04	262	10/19/1998	4:00	390	MC	-17.3	18	-112	N22W01
11/05/1998	20:44	1118	11/09/1998	1:00	450	MC	-18.5	12	-149	N22W18
09/20/1999	6:06	604	09/22/1999	19:00	530	EJ	-15.8	11	-173	S20W05
02/10/2000	2:30	944	02/12/2000	12:00	540	MC	-16.4	13	-133	N31E04
04/04/2000	16:32	1188	04/07/2000	6:00	560	EJ	-27.3	6	-288	N18W55
07/14/2000	10:54	1674	07/15/2000	19:00	740	MC	-45.3	20	-301	N22W07
08/09/2000	16:30	702	08/12/2000	5:00	580	MC	-28.7	18	-235	N20E12
10/02/2000	20:26	569	10/05/2000	13:00	450	EJ	-17.5	6	-182	S09EOO
10/25/2000	8:26	770	10/28/2000	21:00	380	MC	-15.6	14	-127	N09W63
11/03/2000	18:26	291	11/06/2000	17:00	510	MC	-11.7	20	-159	N02W02
03/28/2001	12:50	427	03/31/2001	5:00	640	EJ	-44.7	33	-387	S10E30
04/10/2001	5:30	2411	04/11/2001	22:00	640	MC	-20.5	14	-271	S23W09
08/14/2001	16:01	618	08/17/2001	20:00	500	EJ	-18.1	11	-105	Nl6W36
09/28/2001	8:54	846	10/01/2001	8:00	490	EJ		9	-148	Nl0El8
10/01/2001	16:50	901	10/21/2001	20:00	460	EJ	-16.4	9	-187	Nl5W29
10/25/2001	15:26	1092	10/29/2001	22:00	360	EJ	-14.5	5	-157	S16W21
11/04/2001	16:35	1810	11/06/2001	12:00	600	EJ	-6.2	7	-292	N06W18
11/22/2001	23:30	1437	11/24/2001	14:00	720	MC	-22.7	14	-221	Sl7W36
03/20/2002	17:06	603	03/24/2002	12:00	450	MC	-9.7	15	-100	Sl7W20
04/15/2002	3:50	720	04/17/2002	16:00	480	MC	-12.8	14	-127	Sl5W01
04/17/2002	8:26	1240	04/20/2002	0:00	500	EJ	-14.7	8	-149	Sl4W34
05/08/2002	13:50	614	05/11/2002	15:00	430	EJ	-16.5	15	-110	Sl2W07
05/22/2002	3:26	1557	05/23/2002	20:00	590	MC	-11.6	11	-109	S30W34
08/16/2002	12:30	1585	08/19/2002	12:00	460	EJ	-9.2	8	-106	Sl4E20
09/05/2002	16:54	1748	09/08/2002	4:00	470	EJ	-15.4	11	-181	N09E28
05/28/2003	0:50	1366	05/30/2003	2:00	600	EJ	-16.3	20	-144	S07W20
08/14/2003	20:06	378	08/18/2003	1:00	450	MC	-15.9	18	-148	S10E02
10/28/2003	11:30	2459	10/29/2003	11:00	1300	MC	-27.1	32	-353	Sl6E08
10/29/2003	20:54	2029	10/31/2003	2:00	800	EJ	-27.1	9	-383	Sl5W02
ll/18/2003	8:50	1660	11/20/2003	10:00	580	MC	-50.9	28	-422	NOOE18
01/20/2004	6:00	965	11/22/2004	8:00	560	EJ	-14.9	12	-130	S13W09
07/25/2004	14:54	1333	07/27/2004	2:00	870	MC	-20.3	16	-170	N08W33
11/07/2004	16:54	1759	11/09/2004	20:00	640	MC	-23.8	14	-263	N09W17
05/13/2005	17:12	1689	05/15/2005	6:00	630	MC	-36.5	15	-247	N12E11
05/26/2005	15:06	586	05/30/2005	1:00	460	EJ	-15.9	15	-113	S11E19
08/22/2005	1:31	1194	08/24/2005	14:00	660	EJ	-42.9	20	-216	SllW54
09/09/2005	19:48	2257	09/11/2005	5:00	900	EJ	-3.2	10	-139	Sl2E67

Table 2. Continued

LASCO CME	Time	CME speed	ICME sta11	Time	ICME speed	ICME type	B_z (nT)	B (nT)	Dst (nT)	CME location
12/13/2006	2:54	1774	12/14/2006	22:00	740	MC	-15.7	13	-162	S06W23
08/04/2011	4:12	1315	08/06/2011	22:00	540	EJ	-19.3	4	-115	N19W36
09/24/2011	12:48	1915	09/26/2011	20:00	580	EJ	-24.l	7	-118	N10E56
10/22/2011	5:00	1005	10/24/2011	22:00	460	MC	-13.l	21	-147	N25W77
03/07/2012	0:24	2684	03/09/2012	3:00	550	EJ	-11.2	7	-145	N17E27
07/12/2012	16:48	885	07/15/2012	6:00	490	MC	-18.7	16	-139	S15W01
09/28/2012	0:00	947	10/01/2012	0:00	370	MC	-19.2	14	-122	N06W34
03/15/2013	7:12	1063	03/17/2013	15:00	520	MC	-11.5	9	-132	Nl1El2
03/15/2015	2:36	719	03/17/2015	13:00	560	MC	-17.3	20	-223P	S22W25
06/21/2015	2:36	1366	06/23/2015	2:00	610	EJ	-22.2	14	-204P	Nl2El6
12/16/2015	9:24	579	12/20/2015	3:00	400	MC	-16.8	15	-155P	S13W04
12/28/2015	12:12	1212	12/31/2015	17:00	440	MC	-15.8	10	-110P	S23W11
09/06/2017	12:24	1571	09/8/2017	11:00	590	EJ	-24.2	7	-122P	S08W33

3.3 ICME Transit Time from the Sun to 1 AU

The study examines over 53 distinct, non-recurring GMSs of intensities $Dst \leq -100$ nT, which are reliably associated with halo CMEs and ICMEs. The transit time of an ICME (TICME) is calculated by taking the difference between the time when the CME first appears in the LASCO C2 field of view and the time when the ICME reaches the region near Earth at 1 AU. In Figure 3, we have plotted the transit time of all ICMEs against the initial speed of the correspond-

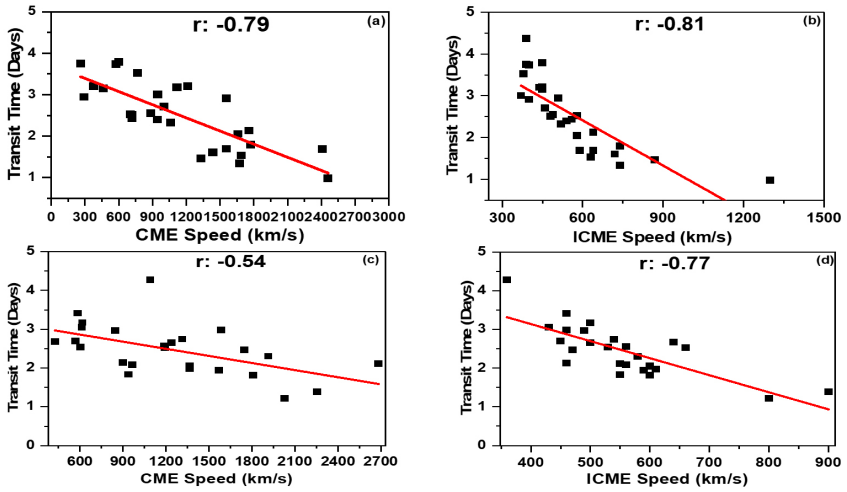


Figure 3. Relationships between the initial halo CME and ICME speeds and the observed ICME transit-times during SC 23 and 24 for MC (a,b) and EJ (c,d) respectively.

ing CME and speed of ICME during SC 23 and 24. During SC 23, the transit time varied between approximately 104 and 23 hours. However, for SC 24, the minimum transit time was significantly higher, around 43 hours. This can be attributed to the fewer high-speed CME events during SC 24, resulting in a majority of ICMEs exhibiting longer Sun-Earth transit times. The goal is to gain a comprehensive understanding of the relationship between the transit time of ICMEs from the Sun to Earth (TICME) and the maximum intensity of the GMS, as measured by the Dst index. The linear regression for ICME transit time versus initial CME and ICME speed separately for MC and EJ types, during SC 23 and SC 24 are represented by the following equations, respectively:

$$\text{For MC} \qquad T_{\text{ICME}} = 3.90 - 1.6V_{\text{CME}} \times 10^{-4} \tag{1}$$

$$T_{\text{ICME}} = 4.79 - 5.1V_{\text{CME}} \times 10^{-4} \tag{2}$$

$$\text{For EJ} \qquad T_{\text{ICME}} = 3.49 - 7.97V_{\text{CME}} \times 10^{-4} \tag{3}$$

$$T_{\text{ICME}} = 4.93 - 7.1V_{\text{CME}} \times 10^{-4} \tag{4}$$

From the analysis, we observe that SC 23 displays a more systematic pattern of variations in CME initial speeds with ICME transit times, compared to the subsequent cycle. During the examination period, we do not find any EJs with speeds exceeding 1000 km/s. When examining the correlation between the transit time of ICME (both MC and EJ) and the speed of CME and ICME, it is observed that the transit time of ICME (TICME) for both MC and EJ exhibit a stronger correlation with the speed of ICME (V_{ICME}), with correlation coefficients of -0.81 and -0.77, respectively. On the contrary, EJ exhibits a moderate correlation with the speed of CME (V_{CME}) with a correlation coefficient of -0.54, whereas MC exhibits a more robust correlation with a coefficient of -0.77. We found that there is a general pattern of decreasing transit times for ICMEs in relation to the initial speeds of CMEs.

These results indicate that the ICME speed near 1 AU is a better predictor of transit time than the initial CME speed, particularly for EJs, where greater propagation-related deceleration and interaction with the ambient solar wind may introduce additional variability. SC 23 shows a more systematic dependence of transit time on the initial CME speed than SC 24. No EJ events with speeds exceeding 1000 km/s were observed during the study period. Although the overall trend indicates decreasing transit time with increasing CME or ICME speed, substantial scatter is present for a given initial CME speed. This variability demonstrates that ICME propagation is not governed solely by the initial CME speed but is also influenced by aerodynamic drag, interaction with the ambient solar wind, CME expansion, and interactions with preceding solar-wind structures. Thus, the transit-time analysis provides evidence that the initial CME kinematics are important but do not uniquely determine the subsequent Sun–Earth propagation profile. The observed correlations are broadly consistent with previous studies reporting an inverse relationship between CME/ICME

speed and Sun–Earth transit time. These findings align with previous research conducted by several authors [13, 14].

3.4 Relationship Between ICME parameters and the intensity of the geomagnetic storms

Research has confirmed that ICMEs are the primary cause of significant geomagnetic storms ($Dst \leq -100$ nT) [15, 16]. CMEs that originate from the Sun are fundamentally magnetic structures that possess substantial magnetic field strengths. These CMEs compress any IMF in their leading regions as they traverse the IP medium and interact with other ICMEs or the surrounding solar wind, causing IP shocks. The southward magnetic field (Bs) present in shock sheaths and ICMEs plays a pivotal role in the generation of geomagnetic storms. It is important to note that for CMEs to cause geomagnetic storms, they must originate near the disk center of the Sun to reach Earth. The majority of these CMEs have been observed as halo CMEs. The characteristics of halo CMEs and geoeffective CMEs are nearly identical [17]. This is primarily due to the fact that the majority of front-side halos are responsible for triggering geomagnetic storms. Although post-event analysis reveals a strong link between halo CMEs and geomagnetic storms, our ability to predict the occurrence and intensity of geomagnetic storms based on halo CME observations remains limited.

The goal is to gain a comprehensive understanding of the relationship between the transit time of ICMEs from the Sun to Earth (TICME) and the maximum intensity of the GMS, as measured by the Dst index. The large number of events analyzed and their distribution on a TICME – Dst plane confirm and significantly enhance known patterns. MC events are marked by a shorter transit time (TICME $\approx$ 1-–4 days) and much more potent GMSs compared to EJ events (TICME $\approx$ 1.5-–4.5 days), with $Dst \leq$ ˇ100 nT. From Figure 4(a,b) shows the relationships between the Dst index and the observed ICME transit-time. The MC exhibits a high correlation with the transit time of ICME, with a correlation coefficient of 0.64. However, it demonstrates a low correlation for EJ, where

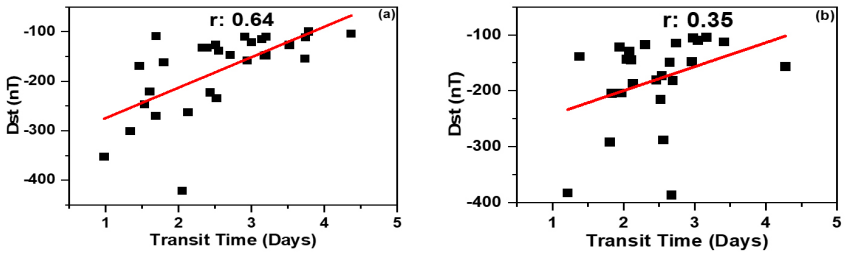


Figure 4. Relationships between the Dst index and the observed ICME transit-time during SC 23 and 24 for MC (a) and EJ (b) respectively.

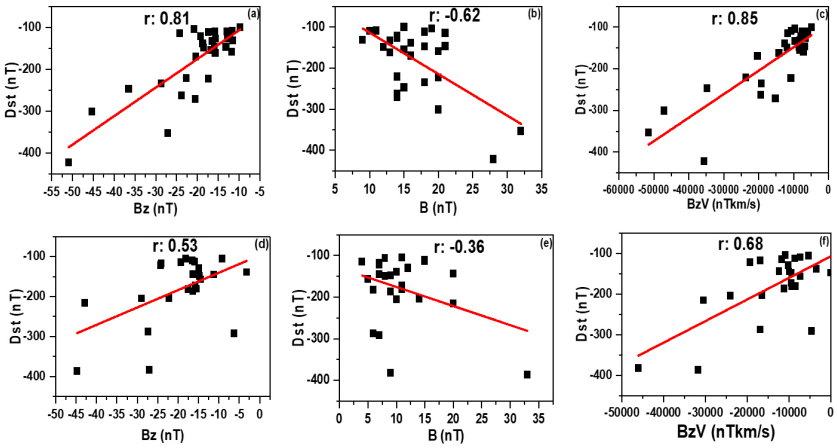


Figure 5. Scatter plots of ICME parameters with Dst. Upper panel (a,b,c) shows the scatter plot of Dst with IMF B_z, IMF B and B_zV for MC; lower panel (d,e,f) shows the scatter plot of IMF B_z, IMF B and B_zV for EJ.

the correlation coefficient is 0.35. For both event types, the shorter the transit time of CMEs/ICMEs, the more intense the GMSs. From the perspective of the nature of GMSs and their solar sources, the findings suggest that both the speed of CMEs/ICMEs and the strength of the magnetic field they carry are largely determined by the parameters of the corresponding eruptions, especially the eruptive magnetic flux and the energy released.

To investigate the possible relationship between the parameters of ICMEs and the intensity of GMSs, a study was conducted comparing ICME parameters with the Dst minimum. The results are displayed in Figure 5. The upper and lower panels of Figure 5, illustrate scatter plots demonstrating the relationship between ICME parameters (IMF B_z, IMF B and B_zV) and the Dst index for MC and EJ respectively. The study found a strong correlation with correlation coefficients of 0.81, -0.62, and 0.85 for MC, while found a moderate correlation with correlation coefficients of 0.53, -0.35 and 0.68 for EJ, respectively. The result confirms that the intensity of geomagnetic storms is influenced by the magnetic field's southward component. Above results were consistent with earlier finding [18, 19].

4 Conclusion

In this study, we performed a statistical analysis of the characteristics of ICMEs during SC 23 and 24 spanning the period 1996 to 2018.The key findings from our statistical analysis are summarized as follows:

1. A significant decrease in the number of ICMEs is observed in SC 24 compared to SC 23. The proportion of MC-type events among the total ICMEs

is significantly higher in SC 24 (64%) compared to SC 23 (41%) whereas other structures (EJ and complex) exhibit a decrease in SC 24.

2. We categorize all 53 halo CME-ICME pair into two distinct subsets, i.e. MCs and EJ that were associated with intense GMS, characterized by a $Dst \leq -100$ nT.
3. The speed range of ICMEs is quite narrow and tends to distribute around the ambient solar wind speed ($\sim$ 400–450 km/s). Most ICME–CME associations correspond to wide CMEs with angular extents of halo CME.
4. During SC 23, the ICME transit time varied between approximately 104 and 23 hours. However, for SC 24, the minimum transit time was significantly higher, around 43 hours.
5. MC and EJ exhibit a stronger correlation with the speed of ICME ($V_{\rm ICME}$), with correlation coefficients of -0.81 and -0.77, respectively. On the contrary, EJ exhibits a moderate correlation with the speed of CME ($V_{\rm CME}$) with a correlation coefficient of -0.54, whereas MC exhibits a more robust correlation with a coefficient of -0.77.
6. The correlation between the Dst index and the observed transit time of ICMEs is high for MCs, (r: 0.64). However, for EJs, the correlation is low, (r: 0.35). For both MCs and EJs, it's observed that shorter transit times of ICMEs correspond to more intense GMSs.
7. The correlation between ICME parameters (IMF B_z, IMF B, and B_zV) and the Dst index was found to be strong for MC, with correlation coefficients of 0.81, -0.62, and 0.85 respectively. However, for EJ, the correlation was moderate, with correlation coefficients of 0.53, -0.35, and 0.68 respectively.

Acknowledgment

Authors would like to thank an anonymous referee for providing fruitful comments and suggestions on the paper. The authors greatly acknowledge the data support provided by SOHO/LASCO CME and ICME catalogue. We are thankful to our college authorities for their help and encouragement.

References

[1] D.F. Webb, T.A. Howard (2012) Coronal Mass Ejections: Observations. *Living Rev. Sol. Phys.* **9**(1) 3.

[2] B. Schmieder, G. Aulanier, B. Vršnak (2015) Flare-CME Models: An Observational Perspective. *Sol. Phys.* **290**(12) 3457–3486.

[3] J. Chen (2017) Physics of erupting solar flux ropes: Coronal mass ejections (CMEs) - Recent advances in theory and observation. *Phys. Plasmas* **24**(9) 090501.

[4] R.F. Wimmer-Schweingruber, et al. (2006) Understanding interplanetary coronal mass ejection signatures: Report of working group B. *Space Sci. Rev.* **123**(1–3) 177–216.

[5] E. Echer, W.D. Gonzalez, B.T. Tsurutani, A.L.C. Gonzalez *2008) Interplanetary conditions causing intense geomagnetic storms ($Dst \leq -100$ nT) during solar cycle 23 (1996-2006). *J. Geophys. Res. Space Phys.* **113**(5) 1–16.

[6] J.T. Gosling, S. Bame, D.J. Mccomas, L. Phillips (1990) Large from bow presentation Alamos plasma experiment events and in which Kp was. *Geophys. Rev. Lett.* **17** 901–904.

[7] L. Burlaga, E. Sittler, F. Mariani, R. Schwenn (1981) Magnetic loop behind an interplanetary shock: Voyager, Helios, and IMP 8 observations. *J. Geophys. Res. Space Phys.* **86**(A8) 6673–6684.

[8] K.P. Dere, G.E. Brueckner, R.A. Howard, D.J. Michels, J.P. Delaboudiniere (1999) LASCO and EIT Observations of Helical Structure in Coronal Mass Ejections. *Astrophys. J.* **516**(1) 465–474.

[9] I.G. Richardson, H.V. Cane (2010) Near-Earth Interplanetary Coronal Mass Ejections During Solar Cycle 23 (1996–2009): Catalog and Summary of Properties. *Sol. Phys.* **264**(1) 189–237.

[10] S. Yashiro, et al. (2004) A catalog of white light coronal mass ejections observed by the SOHO spacecraft. *J. Geophys. Res. Space Phys.* **109**(A7) 1–11.

[11] L. Burlaga, E. Sittler, F. Mariani, R. Schwenn (1981) *J. Geophys. Res. Space Phys.* **86** 6673–6684.

[12] R.-S. Kim, N. Gopalswamy, K.-S. Cho, Y.-J. Moon, S. Yashiro (2013) Propagation Characteristics of CMEs Associated with Magnetic Clouds and Ejecta. *Sol. Phys.* **284**(1) 77–88.

[13] N. Gopalswamy, A. Lara, P.K. Manoharan, R.A. Howard (2005) An empirical model to predict the 1-AU arrival of interplanetary shocks. *Adv. Space Res.* **36**(12) 2289–2294.

[14] M.S. Ibrahim, A. Shanmugaraju, M.B. Lawrance (2015) ScienceDirect Transit time of CME / shock associated with four major geo-effective CMEs in solar cycle 24. *Adv. Space Res.* **55**(1) 407–415.

[15] W.D. Gonzalez, B.T. Tsurutani, A.L. Clúa De Gonzalez (1999) Interplanetary origin of geomagnetic storms. *Space Sci. Rev.* **88**(3–4) 529–562.

[16] J. Zhang, K. Dere, R. Howard, V. Bothmer (2008) Identification of Solar Sources of Major Geomagnetic Storms between 1996 and 2000. *Astrophys. J.* **582** 520.

[17] G. Michalek, N. Gopalswamy, A. Lara, S. Yashiro (2006) Properties and geoeffectiveness of halo coronal mass ejections. *Space Weather* **4**.

[18] C.C. Wu, et al. (2016) The first super geomagnetic storm of solar cycle 24: "The St. Patrick's day event (17 March 2015)". *Earth Planets Space* **68** 151.

[19] H. Dharmashaktu, N.K. Lohani, M. Tewari (2024) *J. Sci. Res.* **16** 355-368.